

Role of Electric Fields on Enhanced Electron Correlation in Surface-Doped FeSe

Young Woo Choi and Hyoung Joon Choi*

Department of Physics, Yonsei University, Seoul 03722, Republic of Korea

(Dated: January 15, 2019)

Electron-doped high- T_c FeSe reportedly has a strong electron correlation that is enhanced with doping. It has been noticed that significant electric fields exist inevitably between FeSe and external donors along with electron transfer. However, the effects of such fields on electron correlation are yet to be explored. Here we study potassium- (K-) doped FeSe layers using density-functional theory combined with dynamical mean-field theory to investigate the roles of such electric fields on the strength of the electron correlation. We find, very interestingly, the electronic potential-energy difference between the topmost Se and Fe atomic layers, generated by local electric fields of ionized K atoms, weakens the Se-mediated hopping between Fe d orbitals. Since it is the dominant hopping channel in FeSe, its reduction narrows the Fe d bands near the Fermi level, enhancing the electron correlation. This effect is orbital dependent and occurs in the topmost FeSe layer only. We also find the K dosing may increase the Se height, enhancing the electron correlation further. These results shed new light on the comprehensive study of high- T_c FeSe and other low-dimensional systems.

Observations of a superconducting T_c as high as 100 K in a monolayer (ML) FeSe/SrTiO₃ (STO) system [1–3] have intensified interest in electron-doped FeSe systems [4–6]. In the FeSe/STO system, electron transfer from the STO substrate to FeSe appears to be a key ingredient for realizing superconductivity [2, 7], and additional electron doping to the system by potassium (K) dosing increases T_c [8]. Moreover, surface doping experiments by K dosing [9–12], Na dosing [13], and liquid gating [14] have shown that electron doping can also increase T_c for bulk, thick-film, and multilayer FeSe.

Along with the enhanced T_c , a common feature shared by electron-doped FeSe systems is that they have much stronger electron correlation than iron pnictides [11, 13, 15–18]. An insulator-superconductor transition was reported in FeSe/STO, which is electron doped interfacially, suggesting strong electron correlation [17]. Strong renormalization of d_{xy} bands was observed, suggesting orbital-dependent electron correlation [18]. Systematic doping experiments with K and Na dosing showed that the correlation strength increases with the doping level [11, 13], which is quite anomalous because the electron correlation usually decreases with deviation from $3d^5$ in Fe-based superconductors [11, 19–21].

An interesting feature is that the electron doping to FeSe is induced usually by charge transfer from external donors such as substrates [7, 22–25] or dosed alkali metals [9–11, 13]. In the viewpoint of electrostatics, such charge transfer is always accompanied by significant electric fields between FeSe and external donors. Thus, not only the doped electrons themselves but also some perturbations from the external donors may possibly affect the electronic structure in FeSe. The presence of such electric fields was noticed previously in the density-functional theory (DFT) calculation [26, 27]; however, their possible importance on the electron correlation is not addressed in any previous theoretical or experimental study.

To study the effects of electric fields from external donors, the simplest prototypical system is K-dosed FeSe. In our present work, we consider K-dosed ML and bilayer (BL) FeSe using DFT combined with the dynamical mean-field theory (DMFT) [28]. We obtain that K dosing induces electron doping only in the first FeSe layer, and K ions generate a strong local electric field near the surface as in other systems [29, 30]. We show, for the first time, that the electric field weakens Se-mediated hopping between Fe $3d$ orbitals, reducing DFT bandwidths of Fe $3d$ near the Fermi level and thereby enhancing the electron correlation. Effects of the electric field are mostly contained in the first FeSe layer, so the second layer is nearly unaffected. These effects, caused by electric fields present generally with external donors, can be ubiquitous in externally electron-doped FeSe, and may happen in other low-dimensional materials. Furthermore, we find the K dosing can increase the Se height (z_{Se}) from the Fe plane, making FeSe layers more correlated.

We performed DFT+DMFT calculations using the all-electron embedded DMFT implementation [31], based on WIEN2k [32]. The electron correlation in Fe $3d$ orbitals is treated within the DMFT, whose validity was well tested for iron pnictides and chalcogenides [33]. The total electron density is determined using the DFT+DMFT charge self-consistency. In the DFT part, we use the local density approximation (LDA) to the exchange-correlation energy [34], and $16 \times 16 \times 1$ k points are sampled in the full Brillouin zone of the unit cell containing two Fe atoms in each FeSe layer, which we call the 2-Fe unit cell hereafter. In the DMFT part, we employ the continuous-time quantum Monte Carlo impurity solver [35] to obtain the local self-energies for the Fe $3d$ orbitals, using $U = 5.0$ eV and $J = 0.8$ eV [36]. These values of U and J , obtained by the self-consistent GW method [37], have been successful in describing various properties of iron pnictides and chalcogenides [36]. We use the nominal double counting correction scheme and the temperature

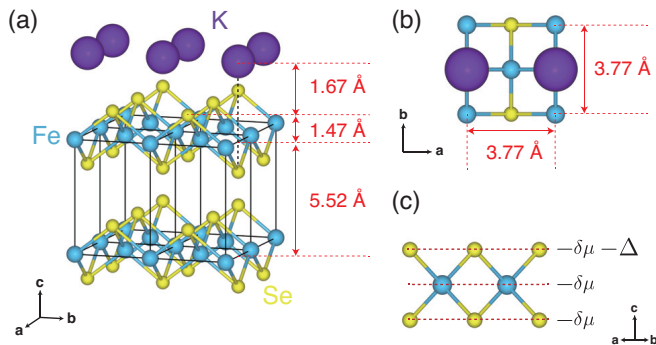


FIG. 1. K-dosed FeSe layer in (a) perspective and (b) top view, where $a = 3.77 \text{ \AA}$ is from experiment of tetragonal bulk FeSe. The optimized Se height is 1.47 \AA for pristine FeSe. K atoms are relaxed while Se atoms are fixed as the pristine case. (c) Schematics of effects of K dosing, where $\delta\mu$ is the overall potential-energy shift in the first FeSe layer and Δ is additional potential-energy change at topmost Se sites.

of 116 K.

The atomic structure of FeSe layers is shown in Fig. 1. Lattice constants are fixed to experimental values of bulk FeSe in the tetragonal phase [Fig. 1(b)]. Then, the chalcogen height is the key structural parameter [38]. When relaxed with LDA, z_{Se} converges to 1.28 \AA for bulk, much smaller than 1.47 \AA in experiment [39]. This discrepancy can be resolved using the DFT+DMFT structural optimization [40]. By minimizing the DFT+DMFT free energy [40], we obtain $z_{\text{Se}} = 1.46 \text{ \AA}$ for bulk paramagnetic (PM) phase, in good agreement with the experiment [39] and previous calculations [36, 40]. This improvement is related to fluctuation of local magnetic moments in the PM phase. For FeSe ML, the optimized z_{Se} slightly increases to 1.47 \AA . For FeSe BL, the distance between Fe layers is set to the experimental value, 5.52 \AA , of bulk FeSe.

After determining the atomic positions of pristine FeSe as described above, we introduce one K atom per 2-Fe unit cell [Figs. 1(a) and 1(b)], and optimize the K-atom height (z_{K}). We define this surface concentration (n_{K}) of K as unity, that is, $n_{\text{K}} = 1$. Then, we reduce n_{K} using the virtual crystal approximation (VCA), where the atomic number of K is reduced to $18 + n_{\text{K}}$ for $n_{\text{K}} > 0$, which is suitable for describing K atoms randomly distributed on the surface as observed experimentally [12]. For the pristine case of $n_{\text{K}} = 0$, we simply do not introduce any K atom. We checked the validity of our VCA carefully by comparing it with ordinary supercell calculations (See the Supplemental Material [41] for the detailed comparison). In most of the following parts of our present work, we will focus on direct electrical effects of the K dosing on the electron correlation by fixing $z_{\text{Se}} = 1.47 \text{ \AA}$ independently of n_{K} . Then, at the last part, we will consider the dependence of z_{Se} on n_{K} [47] and its effect on the electron correlation.

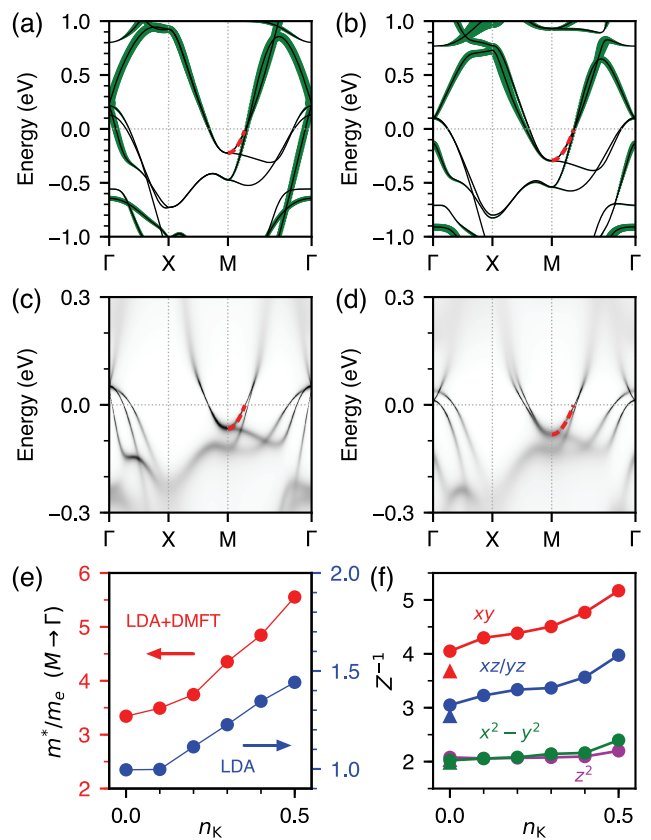


FIG. 2. Electronic structure of FeSe ML. (a),(b) LDA bands (a) without K dosing and (b) with $n_{\text{K}} = 0.3$. Red dashed lines are quadratic fits to bands along $M \rightarrow \Gamma$. The thickness of green solid lines represents Se atomic characters of each state. (c),(d) LDA+DMFT spectral functions (c) without K dosing and (d) with $n_{\text{K}} = 0.3$. Red dashed lines are quadratic fits to maximal points of spectral functions. (e) Effective mass of the electron band at M . (f) Inverse of the quasiparticle weights Z for Fe 3d orbitals. Z^{-1} represents the mass enhancement due to electron correlation. Triangles are Z^{-1} in bulk FeSe.

First, we investigate charge transfer and the electrostatic potential after K dosing on the FeSe bilayer. Our LDA results (Fig. S2 [41]) show that the transferred charge from K is contained within the first FeSe layer, and the strong electric field appears due to ionized K atoms, which is screened by the first FeSe layer, leaving the remaining second FeSe layer almost unaffected because each FeSe layer is metallic. It can be generalized to any multilayer (see Fig. S3 [41] for four layer). Thus, the essential effects of K dosing are (i) potential-energy lowering by $\delta\mu$ at the topmost FeSe layer with respect to the chemical potential to accommodate electrons from K and (ii) additional potential-energy lowering by Δ at the topmost Se atoms with respect to underlying Fe atoms [Fig. 1(c)]. We will use these two parameters, $\delta\mu$ and Δ , to analyze the electronic structure of K-dosed FeSe layers.

Figures 2(a) and 2(b) show our LDA band structures

of pristine and K-dosed (with $n_K = 0.3$) FeSe MLs, respectively. We notice that in the K-dosed ML, bands are shifted downward in energy due to electron doping from the K atom, and Fe $3d$ bands near the Fermi level are narrower than those in the pristine one. While states near the Fermi level have mostly Fe $3d$ character, some of them also have appreciable Se-atom weight as denoted by the thickness of green lines in Figs. 2(a) and 2(b). This Se-atom weight reflects Se-mediated indirect hopping of Fe $3d$ electrons. These states with larger Se weights are lowered more in energy after K dosing because of the K-induced change of the electrostatic potential energy at the topmost Se atomic sites, denoted by $-\Delta$ in Fig. 1(c), in addition to overall potential energy change by $-\delta\mu$. Especially, the hole band having the largest Se weight among the three hole bands at Γ is so sensitive to K dosing that its maximum moves even below the Fermi level. As for electron bands near M , we observe a gradual decrease of bandwidths and increase of LDA effective masses (m^{LDA}). In particular, m^{LDA} of an electron band along the Γ direction is obtained by a quadratic curve fit as marked with red dashed lines in Figs. 2(a) and 2(b). As shown in Fig. 2(e), obtained m^{LDA} in a pristine ML is close to the electron mass (m_e) at vacuum and increases more than 40% with K dosing of $n_K = 0.5$.

For the detailed analysis of K-dosing effects, we performed tight-binding (TB) calculations. First, we constructed a TB Hamiltonian by applying maximally localized Wannier functions [48] to the LDA band structure of pristine FeSe ML. Then, we added $\delta\mu$ and Δ to our TB Hamiltonian and obtained a TB band structure, which agrees well with LDA result of K-dosed FeSe ML. We found that while $\delta\mu$ shifts band energies rigidly, reflecting the electron doping, an increase of Δ reduces bandwidths of Fe $3d$ bands and increases the effective mass of the electron band at the M point (Fig. S4 in Ref. [41]). To understand why Δ affects the bandwidth, we need to focus on the hopping mechanism in FeSe. Because of the small spatial extent of Fe $3d$ orbitals, direct inter-site hoppings are relatively weak. Instead, the dominant hopping channel for Fe $3d$ orbitals is indirect hopping mediated by Se $4p$ orbitals [36]. Since the indirect hopping is the second-order process, its strength is inversely proportional to the energy difference between Fe $3d$ and Se $4p$ orbitals. Thus, the increase of Δ , which makes Fe $3d$ and Se $4p$ more separated in energy by lowering the Se $4p$ energy, results in effectively reduced hopping between Fe $3d$ orbitals.

We performed LDA+DMFT calculations for pristine and K-dosed FeSe MLs, and obtained electronic structures as shown in Figs. 2(c) and (d), respectively. We notice the electron correlation strongly renormalizes LDA band structures so that the bandwidths are shrunk by more than a factor of 3 in our LDA+DMFT calculations. Because of the reduced hopping between Fe d orbitals described above, the electron correlation becomes much

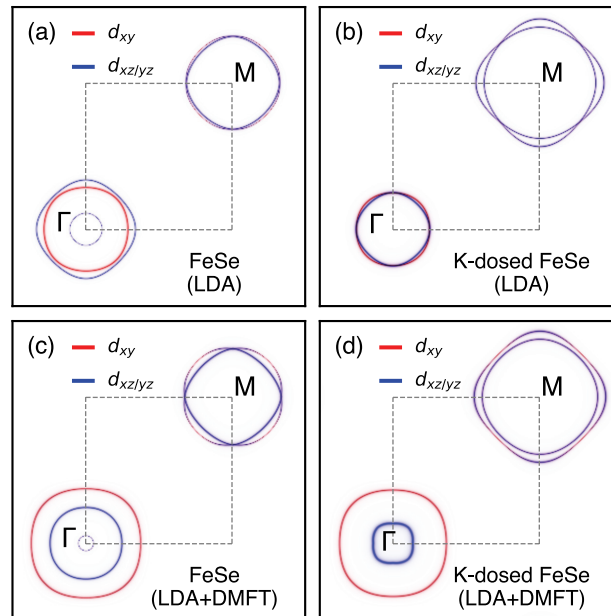


FIG. 3. Fermi surface in FeSe ML. (a),(b) LDA Fermi surfaces (a) without K dosing and (b) with $n_K = 0.3$. (c),(d) Zero-frequency LDA+DMFT spectral functions $A(\mathbf{k}, \omega = 0)$ for pristine and K-dosed cases. Blue and red colors represent d_{xy} and $d_{xz/yz}$ orbital characters, respectively.

stronger for K-dosed FeSe ML. For the direct comparison with LDA results, we fit the maxima of the LDA+DMFT spectral functions [red lines in Figs. 2(c) and 2(d)] to extract the LDA+DMFT effective mass ($m^{\text{LDA+DMFT}}$). Figure 2(e) shows that $m^{\text{LDA+DMFT}}$ increases over 60% as n_K increases to 0.5, and these values are comparable to the experimental observations [11, 13].

The strength of electron correlation can be quantified with the DMFT mass enhancement factor (Z^{-1}), which is the inverse of the quasiparticle weight, $Z^{-1} = 1 - \frac{\partial \text{Re}\Sigma}{\partial \omega} \Big|_{\omega \rightarrow 0}$, where Σ is the DMFT self-energy. In Fig. 2(f), we show the orbital-resolved DMFT mass enhancement factors for K-dosed FeSe ML increase with n_K , indicating that the K dosing makes FeSe more correlated. We notice t_{2g} orbitals are more affected by K dosing and, especially, d_{xy} electrons come to have an extremely strong correlation, with $Z^{-1} > 5$ for $n_K = 0.5$.

Figure 3 shows how the K dosing and the electron correlation modify the Fermi surface of FeSe ML. Figures 3(a) and 3(b) show the LDA Fermi surfaces before and after K dosing, respectively. Two of the three hole pockets around Γ are of $d_{xz/yz}$ characters and the other one is of d_{xy} . We note that the innermost hole pocket has appreciable weights from Se $4p$ orbitals so that it largely shifts below the Fermi level after K dosing. Figures 3(c) and 3(d) show the LDA+DMFT Fermi surfaces before and after K dosing, respectively. Although electron correlation does not alter the number of Fermi-

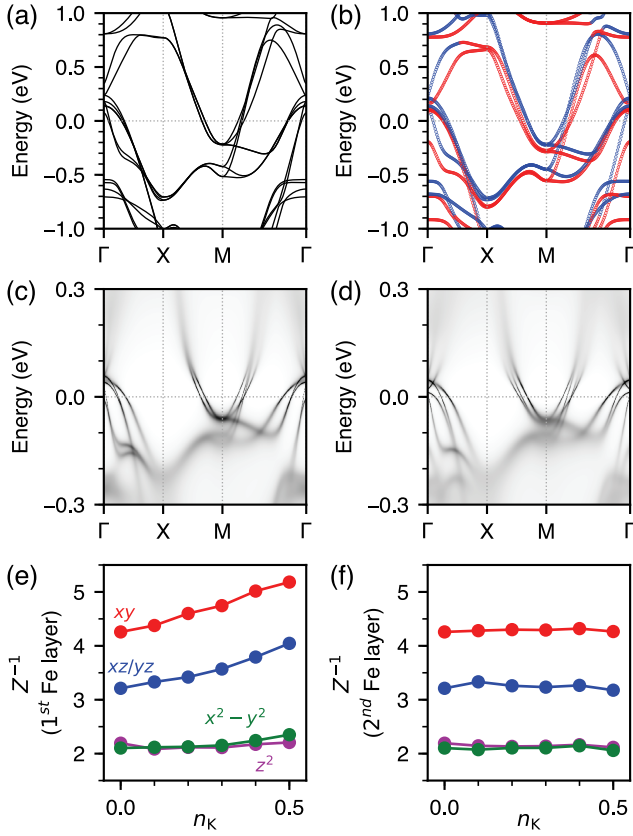


FIG. 4. Electronic structure of FeSe BL. (a),(b) LDA bands (a) without K dosing and (b) with $n_K = 0.3$. Red (blue) circles are states with more weights in the first (second) layer. (c),(d) LDA+DMFT spectral functions (c) without K dosing and (d) with $n_K = 0.3$. (e),(f) DMFT mass enhancement factors of Fe $3d$ orbitals in the first and second FeSe layer.

surface pockets, it distinguishes d_{xy} and $d_{xz/yz}$ orbitals, that is, the d_{xy} hole pocket expands, while $d_{xz/yz}$ hole pockets shrink due to the electron correlation. Two electron pockets around M have mixed orbital characters of d_{xy} and $d_{xz/yz}$. Upon K dosing, the size of electron pockets is enlarged as a result of the combined effects of both the electron doping and the increased effective masses.

Now, we consider the FeSe bilayer. Figures 4(a) and 4(b) show our LDA band structure calculations of pristine FeSe BL and K-dosed FeSe BL with $n_K = 0.3$, respectively. The band structure of pristine FeSe BL [Fig. 4(a)] is qualitatively the same as two sets of monolayer bands split by small interlayer coupling. Before K dosing, all the states near the Fermi level have equal weights at both the first and second layer due to the crystal symmetry. However, they are distinguished after K dosing, as shown in Fig. 4(b), where states with more weights in the first (second) FeSe layer are colored red (blue). We notice that the K dosing affects only the states from the first FeSe layer, consistent with previous DFT study [27] and experiment [11]. Similarly to FeSe ML, the K dosing lowers the energy of first-layer states

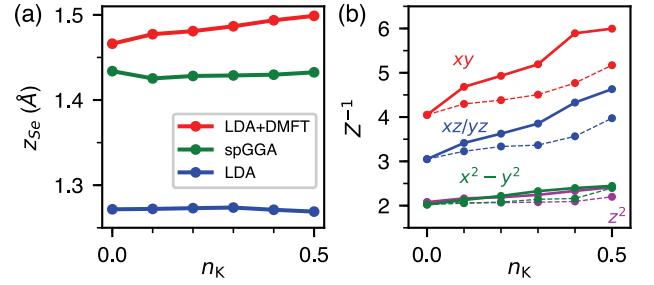


FIG. 5. (a) Se heights (z_{Se}) in FeSe ML optimized at each n_K using different methods. (b) DMFT mass enhancement factors (Z^{-1}) in FeSe ML. Solid lines are Z^{-1} calculated with z_{Se} optimized at each n_K using LDA+DMFT. Dashed lines are Z^{-1} with z_{Se} fixed to the pristine value, as shown in Fig. 2(f).

and reduces their bandwidths, compared with the pristine BL case. With LDA+DMFT [Figs. 4(c) and 4(d)], band dispersions are strongly renormalized by electron correlation, and states from the first and the second layer are split in energy after K dosing. As clearly shown in Figs. 4(e) and 4(f), the DMFT mass enhancements of Fe $3d$ orbitals at the first layer increase with n_K , while those at the second layer remain almost constant.

So far we have focused on the direct electrical effects of K dosing on the electron correlation in FeSe layers by using the same atomic positions independently of n_K . Since the strength of electron correlation in FeSe is very sensitive to z_{Se} [25, 36, 40], we investigate whether the K dosing can change z_{Se} and thereby affect the electron correlation additionally. As shown in Fig. 5(a), our LDA+DMFT calculations predict that the optimized z_{Se} gradually increases with K dosing. While z_{Se} is 1.47 Å for the pristine case, it increases to 1.50 Å with K dosing of $n_K = 0.5$. Since higher z_{Se} makes Fe $3d$ electrons more localized, the increase of z_{Se} with K dosing enhances the electron correlation further as shown in Fig. 5(b). We also find that the increase of z_{Se} is mostly due to the enhanced electron correlation, which is captured by DMFT, rather than the direct electrostatic interaction between FeSe and K, because DFT calculations using LDA or the spin-polarized generalized gradient approximation predict nearly constant z_{Se} insensitively to n_K .

In conclusion, our results show that K-dosed FeSe layers have stronger electron correlation than pristine ones because the change in the electrostatic potential at the topmost Se atoms reduces Fe $3d$ bandwidths by weakening the Se-mediated hopping. This enhancement of electron correlation, which occurs in the topmost FeSe layer only, is indicated by the increased effective masses and reduced quasiparticle weights at the Fermi energy. Furthermore, the K dosing can increase the Se height, which enhances the electron correlation further. These results shed a new light on comprehensive understanding of high- T_c FeSe and can be generalized to other low-dimensional

systems with surface, interface, or gate doping.

This work was supported by NRF of Korea (Grant No. 2011-0018306). Y. W. C. acknowledges support from NRF of Korea (Global Ph.D. Fellowship Program NRF-2017H1A2A1042152). Computational resources have been provided by KISTI Supercomputing Center (Project No. KSC-2017-C3-0079).

* h.j.choi@yonsei.ac.kr

- [1] Q.-Y. Wang, Z. Li, W.-H. Zhang, Z.-C. Zhang, J.-S. Zhang, W. Li, H. Ding, Y.-B. Ou, P. Deng, K. Chang, J. Wen, C.-L. Song, K. He, J.-F. Jia, S.-H. Ji, Y.-Y. Wang, L.-L. Wang, X. Chen, X.-C. Ma, and Q.-K. Xue, Interface-induced high-temperature superconductivity in single unit-cell FeSe films on SrTiO₃, *Chin. Phys. Lett.* **29**, 037402 (2012)
- [2] S. He *et al.*, Phase diagram and electronic indication of high-temperature superconductivity at 65 K in single-layer FeSe films, *Nat. Mater.* **12**, 605 (2013).
- [3] J.-F. Ge, Z.-L. Liu, C. Liu, C.-L. Gao, D. Qian, Q.-K. Xue, Y. Liu, and J.-f. Jia, Superconductivity above 100 K in single-layer FeSe films on doped SrTiO₃, *Nat. Mater.* **14**, 285 (2015).
- [4] X. Liu, L. Zhao, S. He, J. He, D. Liu, D. Mou, B. Shen, Y. Hu, J. Huang, and X. J. Zhou, Electronic structure and superconductivity of FeSe-related superconductors, *J. Phys.: Condens. Matter* **27**, 183201 (2015).
- [5] D. Huang and J. E. Hoffman, Monolayer FeSe on SrTiO₃, *Annu. Rev. Condens. Matter Phys.* **8**, 311 (2017).
- [6] Z. Wang, C. Liu, Y. Liu, and J. Wang, High-temperature superconductivity in one-unit-cell FeSe films, *J. Phys.: Condens. Matter* **29**, 153001 (2017).
- [7] S. Tan, Y. Zhang, M. Xia, Z. Ye, F. Chen, X. Xie, R. Peng, D. Xu, Q. Fan, H. Xu, J. Jiang, T. Zhang, X. Lai, T. Xiang, J. Hu, B. Xie, and D. Feng, Interface-induced superconductivity and strain-dependent spin density waves in FeSe/SrTiO₃ thin films, *Nat. Mater.* **12**, 634 (2013).
- [8] X. Shi, Z. Q. Han, X. L. Peng, P. Richard, T. Qian, X. X. Wu, M. W. Qiu, S. C. Wang, J. P. Hu, Y. J. Sun, and H. Ding, Enhanced superconductivity accompanying a Lifshitz transition in electron-doped FeSe monolayer, *Nat. Commun.* **8**, 14988 (2017).
- [9] C. Tang, D. Zhang, Y. Zang, C. Liu, G. Zhou, Z. Li, and C. Zheng, Superconductivity dichotomy in K-coated single and double unit cell FeSe films on SrTiO₃, *Phys. Rev. B* **92**, 180507 (2015).
- [10] Y. Miyata, K. Nakayama, K. Sugawara, T. Sato, and T. Takahashi, High-temperature superconductivity in potassium-coated multilayer FeSe thin films, *Nat. Mater.* **14**, 775 (2015).
- [11] C. H. P. Wen, H. C. Xu, C. Chen, Z. C. Huang, X. Lou, Y. J. Pu, Q. Song, B. P. Xie, M. Abdel-Hafiez, D. A. Chareev, A. N. Vasiliev, R. Peng, and D. L. Feng, Anomalous correlation effects and unique phase diagram of electron-doped FeSe revealed by photoemission spectroscopy, *Nat. Commun.* **7**, 10840 (2016).
- [12] C.-L. Song, H.-M. Zhang, Y. Zhong, X.-P. Hu, S.-H. Ji, K. He, X.-C. Ma, and Q.-K. Xue, Observation of Double-Dome Superconductivity in Potassium-Doped FeSe Thin Films, *Phys. Rev. Lett.* **116**, 157001 (2016).
- [13] J. J. Seo, B. Y. Kim, B. S. Kim, J. K. Jeong, J. M. Ok, J. S. Kim, J. D. Denlinger, S. K. Mo, C. Kim, and Y. K. Kim, Superconductivity below 20 K in heavily electron-doped surface layer of FeSe bulk crystal, *Nat. Commun.* **7**, 11116 (2016).
- [14] B. Lei, J. H. Cui, Z. J. Xiang, C. Shang, N. Z. Wang, G. J. Ye, X. G. Luo, T. Wu, Z. Sun, and X. H. Chen, Evolution of High-Temperature Superconductivity from a Low- T_c Phase Tuned by Carrier Concentration in FeSe Thin Flakes, *Phys. Rev. Lett.* **116**, 077002 (2016).
- [15] W. L. Yang, A. P. Sorini, C.-C. Chen, B. Moritz, W.-S. Lee, F. Vernay, P. Olalde-Velasco, J. D. Denlinger, B. Delley, J.-H. Chu, J. G. Analytis, I. R. Fisher, Z. A. Ren, J. Yang, W. Lu, Z. X. Zhao, J. van den Brink, Z. Hussain, Z.-X. Shen, and T. P. Devereaux, Evidence for weak electronic correlations in iron pnictides, *Phys. Rev. B* **80**, 014508 (2009).
- [16] M. M. Qazilbash, J. J. Hamlin, R. E. Baumbach, L. Zhang, D. J. Singh, M. B. Maple, and D. N. Basov, Electronic correlations in the iron pnictides, *Nat. Phys.* **5**, 647 (2009).
- [17] J. He, X. Liu, W. Zhang, L. Zhao, D. Liu, S. He, D. Mou, F. Li, C. Tang, Z. Li, L. Wang, Y. Peng, Y. Liu, C. Chen, L. Yu, G. Liu, X. Dong, J. Zhang, C. Chen, Z. Xu, X. Chen, X. Ma, Q. Xue, and X. J. Zhou, Electronic evidence of an insulator-superconductor crossover in single-layer FeSe/SrTiO₃ films, *Proc. Natl. Acad. Sci. U.S.A.* **111**, 18501 (2014).
- [18] M. Yi *et al.*, Observation of universal strong orbital-dependent correlation effects in iron chalcogenides, *Nat. Commun.* **6**, 7777 (2015).
- [19] L. de' Medici, G. Giovannetti, and M. Capone, Selective Mott Physics as a Key to Iron Superconductors, *Phys. Rev. Lett.* **112**, 177001 (2014).
- [20] A. Georges, L. de' Medici, and J. Mravlje, Strong correlations from Hund's coupling, *Annu. Rev. Condens. Matter Phys.* **4**, 137 (2013).
- [21] M. Nakajima, S. Ishida, T. Tanaka, K. Kihou, Y. Tomioka, T. Saito, C.-H. Lee, H. Fukazawa, Y. Kohori, T. Kakeshita, A. Iyo, T. Ito, H. Eisaki, and S.-i. Uchida, Strong electronic correlations in iron pnictides: Comparison of optical spectra for BaFe₂As₂-related compounds, *J. Phys. Soc. Jpn.* **83**, 104703 (2014).
- [22] J. Bang, Z. Li, Y. Y. Sun, A. Samanta, Y. Y. Zhang, W. Zhang, L. Wang, X. Chen, X. Ma, Q. K. Xue, and S. B. Zhang, Atomic and electronic structures of single-layer FeSe on SrTiO₃ (001): The role of oxygen deficiency, *Phys. Rev. B* **87**, 220503 (2013).
- [23] K. Zou, S. Mandal, S. D. Albright, R. Peng, Y. Pu, D. Kumah, C. Lau, G. H. Simon, O. E. Dagdeviren, X. He, I. Božović, U. D. Schwarz, E. I. Altman, D. Feng, F. J. Walker, S. Ismail-Beigi, and C. H. Ahn, Role of double TiO₂ layers at the interface of FeSe/SrTiO₃ superconductors, *Phys. Rev. B* **93**, 180506 (2016).
- [24] H. Zhang, D. Zhang, X. Lu, C. Liu, G. Zhou, X. Ma, L. Wang, P. Jiang, Q.-K. Xue, and X. Bao, Origin of charge transfer and enhanced electron-phonon coupling in single unit-cell FeSe films on SrTiO₃, *Nat. Commun.* **8**, 214 (2017).
- [25] S. Mandal, P. Zhang, S. Ismail-Beigi, and K. Haule, How Correlated is the FeSe/SrTiO₃ System?, *Phys. Rev. Lett.* **119**, 067004 (2017).

- [26] F. Zheng, Z. Wang, W. Kang, and P. Zhang, Antiferromagnetic FeSe monolayer on SrTiO₃: The charge doping and electric field effects, *Sci. Rep.* **3**, 2213 (2013).
- [27] F. Zheng, L.-L. Wang, Q.-K. Xue, and P. Zhang, Band structure and charge doping effects of the potassium-adsorbed FeSe/SrTiO₃ system, *Phys. Rev. B* **93**, 075428 (2016).
- [28] G. Kotliar, S. Y. Savrasov, K. Haule, V. S. Oudovenko, O. Parcollet, and C. A. Marianetti, Electronic structure calculations with dynamical mean-field theory, *Rev. Mod. Phys.* **78**, 865 (2006).
- [29] J. Kim, S. S. Baik, S. H. Ryu, Y. Sohn, S. Park, B.-G. Park, J. Denlinger, Y. Yi, H. J. Choi, and K. S. Kim, Observation of tunable band gap and anisotropic Dirac semimetal state in black phosphorus, *Science* **349**, 723 (2015).
- [30] S. S. Baik, K. S. Kim, Y. Yi, and H. J. Choi, Emergence of two-dimensional massless Dirac fermions, chiral pseudospins, and Berry's phase in potassium doped few-layer black phosphorus, *Nano Lett.* **15**, 7788 (2015).
- [31] K. Haule, C.-H. Yee, and K. Kim, Dynamical mean-field theory within the full-potential methods: Electronic structure of CeIrIn₅, CeCoIn₅, and CeRhIn₅, *Phys. Rev. B* **81**, 195107 (2010).
- [32] P. Blaha, K. Schwarz, G. Madsen, D. Kvasnicka, and J. Luitz, *WIEN2k, An Augmented Plane Wave + Local Orbitals Program for Calculating Crystal Properties* (Karlheinz Schwartz, Technische Universität, Wien, Austria, 2001).
- [33] P. Sémon, K. Haule, and G. Kotliar, Validity of the local approximation in iron pnictides and chalcogenides, *Phys. Rev. B* **95**, 195115 (2017).
- [34] J. P. Perdew and Y. Wang, Accurate and simple analytic representation of the electron-gas correlation energy, *Phys. Rev. B* **45**, 13244 (1992).
- [35] K. Haule, Quantum Monte Carlo impurity solver for cluster dynamical mean-field theory and electronic structure calculations with adjustable cluster base, *Phys. Rev. B* **75**, 155113 (2007).
- [36] Z. P. Yin, K. Haule, and G. Kotliar, Kinetic frustration and the nature of the magnetic and paramagnetic states in iron pnictides and iron chalcogenides, *Nat. Mater.* **10**, 932 (2011).
- [37] A. Kutepov, K. Haule, S. Y. Savrasov, and G. Kotliar, Self-consistent GW determination of the interaction strength: Application to the iron arsenide superconductors, *Phys. Rev. B* **82**, 045105 (2010).
- [38] C.-Y. Moon and H. J. Choi, Chalcogen-Height Dependent Magnetic Interactions and Magnetic Order Switching in FeSe_xTe_{1-x}, *Phys. Rev. Lett.* **104**, 057003 (2010).
- [39] T. M. McQueen, Q. Huang, V. Ksenofontov, C. Felser, Q. Xu, H. Zandbergen, Y. S. Hor, J. Allred, A. J. Williams, D. Qu, J. Checkelsky, N. P. Ong, and R. J. Cava, Extreme sensitivity of superconductivity to stoichiometry in Fe_{1+δ}Se, *Phys. Rev. B* **79**, 014522 (2009).
- [40] K. Haule and G. L. Pascut, Forces for structural optimizations in correlated materials within a DFT+embedded DMFT functional approach, *Phys. Rev. B* **94**, 195146 (2016).
- [41] See Supplemental Material for (i) comparison of our virtual crystal approximation of K-dosed FeSe layers and corresponding ordinary supercell calculations, (ii) analysis of electron transfer, electrostatic potential-energy change, and effective electric field induced by K dosing, and (iii) tight-binding analysis of K-dosing effects, which includes Refs. [42–46].
- [42] S. Kim, J. Ihm, H. J. Choi, and Y.-W. Son, Origin of Anomalous Electronic Structures of Epitaxial Graphene on Silicon Carbide, *Phys. Rev. Lett.* **100**, 176802 (2008).
- [43] H. Lee, S. Kim, J. Ihm, Y.-W. Son, and H. J. Choi, Field-induced recovery of massless Dirac fermions in epitaxial graphene on SiC, *Carbon* **49**, 2300 (2011).
- [44] O. Rubel, A. Bokhanchuk, S. J. Ahmed, and E. Assmann, Unfolding the band structure of disordered solids: From bound states to high-mobility Kane fermions, *Phys. Rev. B* **90**, 115202 (2014).
- [45] J. M. Soler, E. Artacho, J. D. Gale, A. Garcia, J. Junquera, P. Ordejón, and D. Sánchez-Portal, The SIESTA method for *ab initio* order-N materials simulation, *J. Phys.: Condens. Matter* **14**, 2745 (2002).
- [46] J. Kune, R. Arita, P. Wissgott, A. Toschi, H. Ikeda, and K. Held, Wien2wannier: From linearized augmented plane waves to maximally localized Wannier functions, *Comp. Phys. Commun.* **181**, 1888 (2010).
- [47] K dosing also causes tiny lateral displacements (less than 0.01 Å) of Fe and Se atoms in the first FeSe layer only, which have negligible effect on the electronic structure.
- [48] A. A. Mostofi, J. R. Yates, G. Pizzi, Y.-S. Lee, I. Souza, D. Vanderbilt, and N. Marzari, An updated version of wannier90: A tool for obtaining maximally-localised Wannier functions, *Comp. Phys. Commun.* **185**, 2309 (2014).

Supplemental Material:
Role of Electric Fields on Enhanced Electron Correlation in Surface-Doped FeSe

Young Woo Choi and Hyoung Joon Choi*

Department of Physics, Yonsei University, Seoul 03722, Korea

(Dated: January 15, 2019)

This supplemental material provides (i) comparison of our virtual crystal approximation of K-dosed FeSe layers and corresponding ordinary supercell calculations, (ii) analysis of electron transfer, electrostatic potential-energy change, and effective electric field induced by K dosing, and (iii) tight-binding analysis of K-dosing effects.

S1. Virtual crystal approximation for K dosing

In our present work, we define the K concentration n_K as the number of K atoms per surface unit cell which contains two Fe atoms in each FeSe layer. We call this surface unit cell as 2-Fe unit cell hereafter. To simulate K-dosed FeSe layers with $n_K < 1$, we use a virtual crystal approximation (VCA) where one K atom is introduced to the 2-Fe unit cell and the atomic number of the K atom is reduced to $18 + n_K$.

To check the validity of our VCA method, we compare the VCA electronic structures of $n_K = 0.25$ and 0.5 cases with ordinary supercell calculations. For $n_K = 0.25$, we introduced one K atom to a 2×2 supercell of FeSe monolayer (ML) and performed ordinary LDA supercell calculation. For clearer comparison, we unfolded the supercell band structure [1–3] and obtained the unfolded LDA band structure as shown in Fig. S1(a). For $n_K = 0.5$, we introduced one K atom to a $\sqrt{2} \times \sqrt{2}$ supercell and obtained the unfolded LDA band structure as shown in Fig. S1(b). Figures S1(c) and (d) show our VCA band structures for $n_K = 0.25$ and 0.5 , respectively. Except for some features arising from the broken translational symmetry in the supercell calculations, our VCA results agree excellently with the supercell results. This supports the validity of our VCA method for K-dosed FeSe layers.

For $n_K > 0.5$, a potassium band becomes so dispersive that it reaches down below the Fermi level, creating a new electron pocket near Γ point. We do not regard this potassium band as fully relevant in a real sample since K atoms are likely to be disordered on the surface and may not form a coherent band. Thus, we limit our present work in the range of $n_K \leq 0.5$

S2. Electrostatic change after K dosing

From self-consistent LDA calculations of FeSe bilayer (BL) with and without K dosing, we analyzed (i) the electron transfer ($\Delta\rho$) from K to FeSe, (ii) change (ΔV_{KS}) in the Kohn-Sham effective potential before and after K dosing, and (iii) the effective electric field ($-\partial(\Delta V_{KS})/\partial z$) generated by K dosing. For these analy-

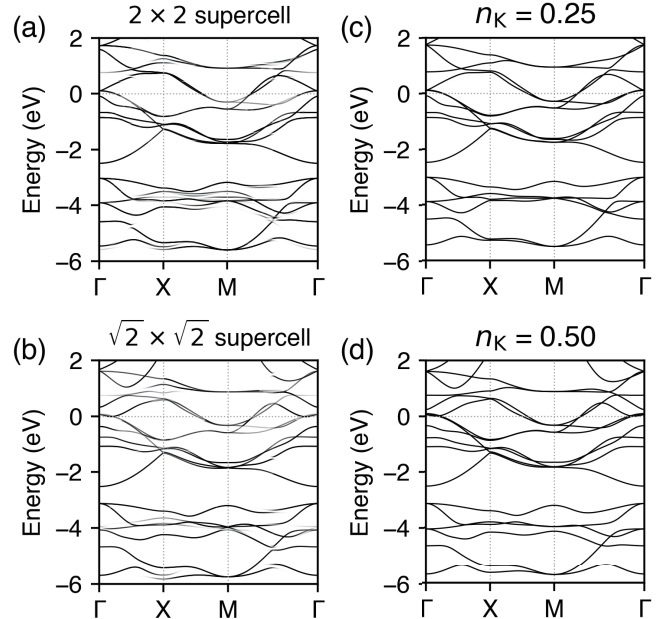


FIG. S1. Comparison of supercell and VCA results for K-dosed FeSe monolayer. (a) Unfolded LDA band structure from the supercell calculation with one K atom per 2×2 supercell corresponding to $n_K = 0.25$. (b) Unfolded LDA band structure from the supercell calculation with one K atom per $\sqrt{2} \times \sqrt{2}$ supercell corresponding to $n_K = 0.5$. (c) VCA band structure with $n_K = 0.25$. (d) VCA band structure with $n_K = 0.5$. In (a)-(d), Γ , X, and M are high-symmetry points of the unit-cell Brillouin zone.

ses, we used the pseudopotential method as implemented in SIESTA [4]. For the K-dosed case, we used $n_K = 1$.

In more detail, we define the electron transfer $\Delta\rho$ as $\Delta\rho = \rho^{\text{K-dosed FeSe BL}} - \rho^{\text{FeSe BL}} - \rho^{\text{K}}$, where $\rho^{\text{K-dosed FeSe BL}}$, $\rho^{\text{FeSe BL}}$, and ρ^{K} are electron distributions in K-dosed FeSe BL, pristine FeSe BL, and one isolated K atom in the same surface unit cell, respectively. Figure S2 shows $\Delta\rho$ averaged in the xy plane and plotted along the z -direction. This plot shows that the electron is transferred from the K atom to the topmost FeSe layer, with negligible electron transfer to the second layer.

We define the change (ΔV_{KS}) in the Kohn-Sham ef-

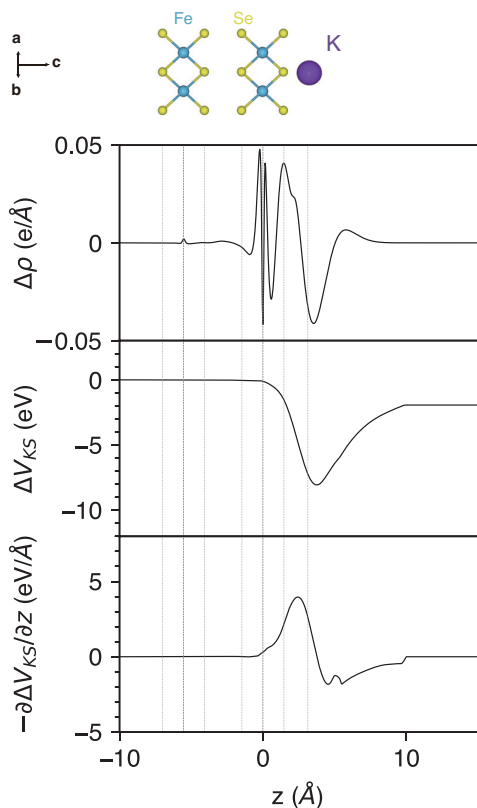


FIG. S2. Electron transfer (top), potential-energy change (middle), and effective electric field (bottom) induced by K dosing, obtained by comparing LDA results of pristine FeSe BL and K-dosed FeSe BL with $n_K = 1$. Vertical lines indicate positions of atomic sites matching with the ball-and-stick model of K-dosed FeSe BL shown on top of the plot. Definitions of $\Delta\rho$, ΔV_{KS} , and $-\partial(\Delta V_{KS})/\partial z$ are given in the text.

fective potential before and after K dosing as $\Delta V_{KS} = V_{KS}^{\text{K-dosed FeSe BL}} - V_{KS}^{\text{FeSe BL}}$, where $V_{KS}^{\text{K-dosed FeSe BL}}$ and $V_{KS}^{\text{FeSe BL}}$ are self-consistent Kohn-Sham effective potentials in K-dosed and pristine FeSe BLs, respectively. Figure S2 shows ΔV_{KS} averaged in the xy plane and plotted along the z -direction. We notice that the K dosing generates significant potential-energy difference between Fe and Se atom sites in the topmost FeSe layer, while it slightly lowers the potential energy of Fe atom sites in the topmost FeSe layer.

Finally, we consider $-\partial(\Delta V_{KS})/\partial z$ as indicating the effective electric field generated by K dosing. Figure S2 shows $-\partial(\Delta V_{KS})/\partial z$ averaged in the xy plane and plotted along the z -direction. We notice that a strong electric field is generated near the topmost surface Se atom site.

In order to show more clearly that only the first FeSe layer is affected by dosed K atoms, we also considered FeSe four-layer instead of FeSe bilayer. As shown in Fig. S3, only the topmost FeSe layer closest to K atoms is affected as in the case of FeSe bilayer while all the other three FeSe layers are almost unaffected.

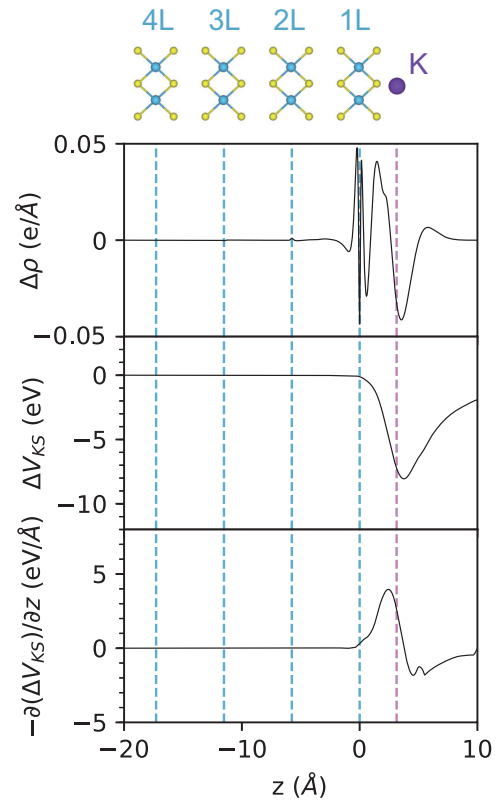


FIG. S3. Electron transfer (top), potential-energy change (middle), and effective electric field (bottom) induced by K dosing, obtained by comparing LDA results of pristine FeSe four-layer and K-dosed FeSe four-layer with $n_K = 1$. $\Delta\rho$, ΔV_{KS} , and $-\partial(\Delta V_{KS})/\partial z$ are defined similarly to the bilayer case. Vertical dashed lines indicate positions of Fe and K atomic sites matching with the ball-and-stick model of K-dosed FeSe four-layer shown on top of the plot.

S3. Tight-binding analysis of K-dosing effects

We construct a tight-binding (TB) model including all Fe $3d$ and Se $4p$ orbitals using the maximally localized Wannier functions [5, 6]. Figures S4(a) and (b) show LDA and TB band structures of the pristine FeSe ML, respectively. The TB bands agree well with the LDA results. This supports the validity of our TB model.

In K-dosed FeSe layers, effects of K dosing can be described by two changes in the TB Hamiltonian. One is the overall lowering (by $\delta\mu$) of the potential energy in the first FeSe layer with respect to the second FeSe layer, and the other is the additional lowering (by Δ) of the potential energy at the topmost Se atom site with respect to the Fe atom site in the first FeSe layer. These two parameters, $\delta\mu$ and Δ , capture essential features of the electronic structure of K-dosed FeSe systems. The lowering $\delta\mu$ brings surface electron doping to the system, and the lowering Δ accounts for the Fe bandwidth reduction by weakening Se-mediated hopping between Fe orbitals.

Figure S4(c) shows LDA band structure for K-dosed

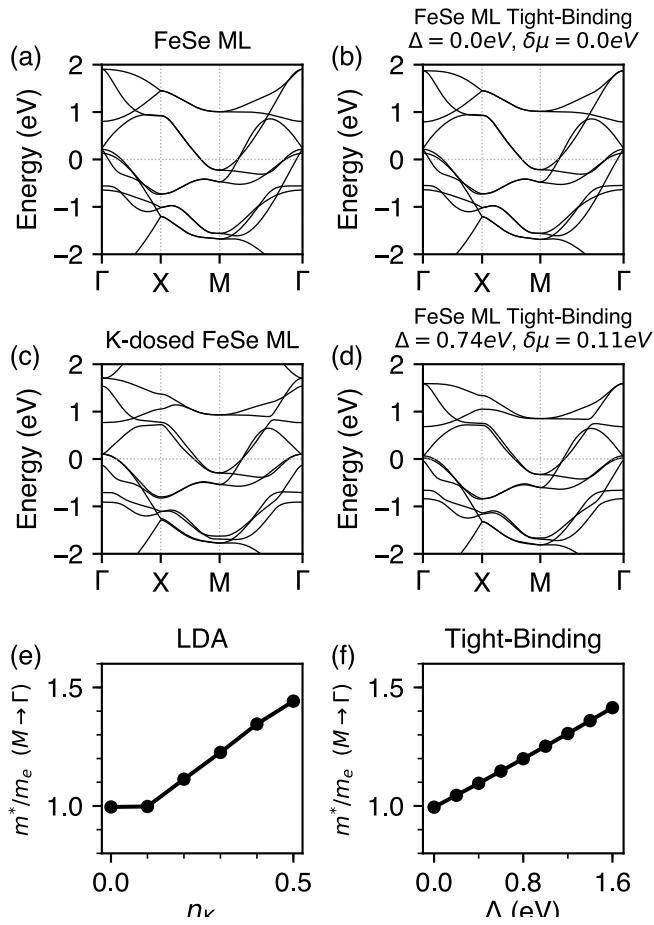


FIG. S4. Comparison of LDA and TB electronic structures. (a) LDA bands for pristine FeSe ML. (b) TB bands for pristine FeSe ML. (c) LDA bands for K-dosed FeSe ML with $n_K = 0.3$. (d) TB bands with $\delta\mu = 0.11 \text{ eV}$ and $\Delta = 0.74 \text{ eV}$ which correspond to $n_K = 0.3$. (e) LDA effective mass of an electron band along M- Γ direction as a function of the K concentration (n_K). (f) TB effective mass of the corresponding electron band along M- Γ direction as a function of Δ . For FeSe ML, $\delta\mu$ shifts the whole TB band structure rigidly.

FeSe ML with $n_K = 0.3$. This LDA band structure can be reproduced by varying $\delta\mu$ and Δ in our TB model [Fig. S4(d)]. As clearly shown in Fig. S4(f), increase of Δ increases the effective mass of the Fe 3d band. This is because the main hopping channel of Fe 3d orbitals is the indirect hopping mediated by Se 4p orbitals and Δ increases the energy separation between Fe 3d and Se 4p orbitals, weakening the indirect hopping.

* h.j.choi@yonsei.ac.kr

- [1] S. Kim, J. Ihm, H. J. Choi, and Y.-W. Son, Origin of anomalous electronic structures of epitaxial graphene on silicon carbide, *Phys. Rev. Lett.* **100**, 176802 (2008).
- [2] H. Lee, S. Kim, J. Ihm, Y.-W. Son, and H. J. Choi, Field-induced recovery of massless Dirac fermions in epitaxial graphene on SiC, *Carbon* **49**, 2300 (2011).
- [3] O. Rubel, A. Bokhanchuk, S. J. Ahmed, and E. Assmann, Unfolding the band structure of disordered solids: From bound states to high-mobility Kane fermions, *Phys. Rev. B* **90**, 115202 (2014).
- [4] J. M. Soler, E. Artacho, J. D. Gale, A. Garcia, J. Junquera, P. Ordejón, and D. Sánchez-Portal, The SIESTA method for ab initio order- N materials simulation, *J. Phys.: Condens. Matter* **14**, 2745 (2002).
- [5] A. A. Mostofi, J. R. Yates, G. Pizzi, Y.-S. Lee, I. Souza, D. Vanderbilt, and N. Marzari, An updated version of wannier90: A tool for obtaining maximally-localised Wannier functions, *Comp. Phys. Commun.* **185**, 2309 (2014).
- [6] J. Kune, R. Arita, P. Wissgott, A. Toschi, H. Ikeda, and K. Held, Wien2wannier: From linearized augmented plane waves to maximally localized Wannier functions, *Comp. Phys. Commun.* **181**, 1888 (2010).